Elsevier Editorial System(tm) for Acta Biomaterialia

Manuscript Draft

Manuscript Number: AB-17-1350

Title: The Hierarchical Response of Human Corneal Collagen to Load

Article Type: Full length article

Keywords: Collagen
cornea
X-ray scattering
biomechanics
microstructure

Corresponding Author: Dr. James Bell, Ph.D.

Corresponding Author's Institution: Cardiff University

First Author: James Bell, Ph.D.

Order of Authors: James Bell, Ph.D.; Sally Hayes; Charles Whitford; Juan Sanchez-Weatherby; Olga Shebanova; Claudio Vergari; C P Winlove; Nick J Terrill; Thomas Sorensen; Ahmed Elsheikh; Keith M Meek

Abstract: Fibrillar collagen in the human cornea is integral to its function as a transparent lens of precise curvature, and its arrangement is now well-characterised in the literature. While there has been considerable effort to incorporate fibrillar architecture into mechanical models of the cornea, the mechanical response of corneal collagen to small applied loads is not well understood. In this study the fibrillar and molecular response to tensile load was quantified using small and wide angle X-ray scattering (SAXS/WAXS), and digital image correlation (DIC) photography was used to calculate the local strain field that gave rise to the hierarchical changes. A molecular scattering model was used to calculate the tropocollagen tilt relative to the fibril axis and changes associated with applied strain. Changes were measured in the D-period, molecular tilt and the orientation and spacing of the fibrillar and molecular networks. These measurements were summarised into hierarchical deformation mechanisms, which were found to contribute at varying strains. The change in molecular tilt is indicative of a sub-fibrillar "spring-like" deformation mechanism, which was found to account for most of the applied strain under physiological and near-physiological loads. This deformation mechanism may explain the greater flexibility of fine collagen fibrils in other tissues, which are known to comprise molecules of high helical tilt, over their thicker counterparts with predominantly straight molecular alignment. Such a mechanism may play an important functional role in tissues rich in fine fibrils, such as skin and cartilage.

Cover Letter

Dr James Bell
School of Optometry and Vision Sciences
Cardiff University
Maindy Road
Cardiff
CF24 4HQ
UK

Dear Prof. Wagner

Please find attached a manuscript entitled “The Hierarchical Response of Human Corneal Collagen to Load”, which the authors wish to be considered for publication in Acta Biomaterialia.

This work presents findings that quantify a subfibrillar deformation mechanism in collagen that has not been reported before, which has significant implications for the understanding of tissue mechanics and changes in disease. The study quantifies the deformation mechanisms in corneal collagen at hierarchies ranging from the molecular to the fibrillar, and presents the findings alongside those from the literature to give a more complete picture of corneal biomechanics.

Given the scope of these findings, we believe this manuscript will be of significant interest to readers with backgrounds in soft tissue or biomaterial mechanics and structure. Furthermore, we include suggestions about how to carry out this type of investigation on any other collagenous material.

Thank you for your consideration.

Best wishes,
James Bell

Graphical Abstract

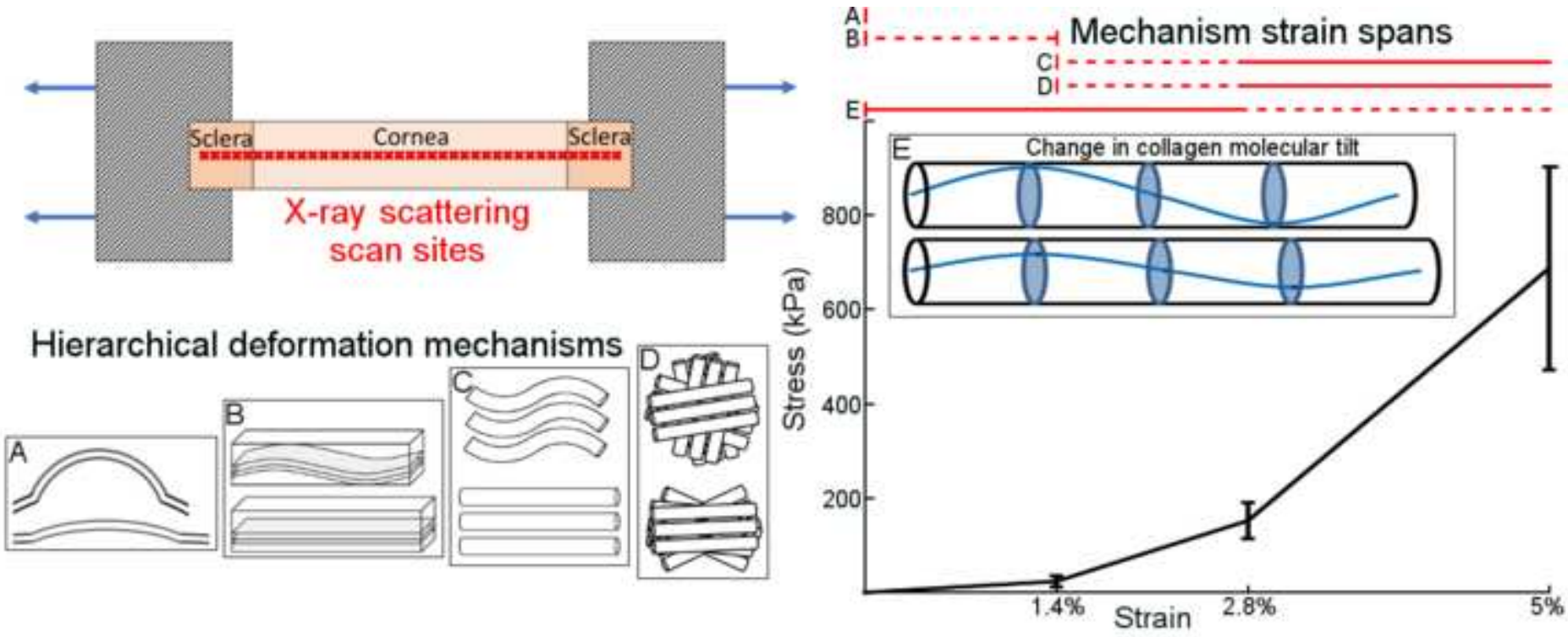

***Statement of Significance**

Statement of Significance

Collagen is the primary mediator of soft tissue biomechanics, and variations in its hierarchical structure convey the varying amounts of structural support necessary for organs to function normally. Here we have examined the structural response of corneal collagen to tensile load using X-rays to probe hierarchies ranging from molecular to fibrillar. We found a previously unreported deformation mechanism whereby molecules, which are helically arranged relative to the axis of their fibril, change in tilt akin to the manner in which a spring stretches. This “spring-like” mechanism accounts for a significant portion of the applied deformation at low strains (<3%). These findings will inform the future design of collagen-based artificial corneas being developed to address world-wide shortages of corneal donor tissue.

The Hierarchical Response of Human Corneal Collagen to Load

J. S. Bell[1,2], S. Hayes[1,2], C. Whitford[3], J. Sanchez-Weatherby[4], O. Shebanova[4], C. Vergari[5], C. P. Winlove[5], N Terrill[4], T. Sorensen[4], A. Elsheikh[3,6], K. M. Meek[1,2].

[1] School of Optometry and Vision Sciences, Cardiff University, Maindy Road, Cathays, Cardiff CF24 4HQ, UK
[2]Cardiff Institute for Tissue Engineering and Repair (CITER), Cardiff University, Wales CF24 4HQ, UK
[3]School of Engineering, University of Liverpool, The Quadrangle, Brownlow Hill, Liverpool L69 3GH, UK
[4]Diamond Light Source Ltd, Diamond House, Harwell Science & Innovation Campus, Didcot, Oxfordshire OX11 0DE, UK
[5]Department of Physics and Astronomy, University of Exeter, Physics Building, Stocker Road, Exeter EX4 4QL, UK
[6]NIHR Biomedical Research Centre for Ophthalmology, Moorfields Eye Hospital NHS Foundation Trust and UCL Institute of Ophthalmology, UK

Corresponding author:
James Bell, School of Optometry and Vision Science, Cardiff University, Maindy Road, Cathays, Cardiff CF24 4HQ, UK
Tel. (+44) 2920 876356
E-mail: bellj10@cardiff.ac.uk

Keywords: Collagen, cornea, X-ray scattering, biomechanics, microstructure

Abstract

Fibrillar collagen in the human cornea is integral to its function as a transparent lens of precise curvature, and its arrangement is now well-characterised in the literature. While there has been considerable effort to incorporate fibrillar architecture into mechanical models of the cornea, the mechanical response of corneal collagen to small applied loads is not well understood. In this study the fibrillar and molecular response to tensile load was quantified using small and wide angle X-ray scattering (SAXS/WAXS), and digital image correlation (DIC) photography was used to calculate the local strain field that gave rise to the hierarchical changes. A molecular scattering model was used to calculate the tropocollagen tilt relative to the fibril axis and changes associated with applied strain. Changes were measured in the D-period, molecular tilt and the orientation and spacing of the fibrillar and molecular networks. These measurements were summarised into hierarchical deformation mechanisms, which were found to contribute at varying strains. The change in molecular tilt is indicative of a sub-fibrillar "spring-like" deformation mechanism, which was found to account for most of the applied strain under physiological and near-physiological loads. This deformation mechanism may explain the greater flexibility of fine collagen fibrils in other tissues, which are known to comprise molecules of high helical tilt, over their thicker counterparts with predominantly straight molecular alignment. Such a mechanism may play an important functional role in tissues rich in fine fibrils, such as skin and cartilage.

Introduction

Collagen is the most abundant structural protein in the mammalian body, and plays a primarily mechanical role in facilitating normal organ processes, whilst conveying structural integrity and resistance to damage and injury. The mechanical environments of each part of the body differ enormously, and it is through variations in the hierarchical structure of collagen and its interactions with cells and the extracellular matrix that these environments are maintained. The mechanical properties of collagen are of great interest, as many degenerative diseases and surgical procedures perturb the collagen network, leading to improper function.

The type I tropocollagen molecule is the basic building block of most collagenous tissues, and consists of three polypeptide chains arranged in a superhelix measuring approximately 280 nm long and 1.5 nm in diameter. It is very stiff, with tensile modulus ranging from 2.9 GPa to in excess of 9 GPa depending upon species and tissue type [1]. Tropocollagen molecules are arranged in a staggered array with a highly ordered offset of 64 – 67 nm, referred to as the D-period [2]. Arrays of molecules form fibrils, which can vary in diameter from 12 nm to over 500 nm [3]. An intermediate structure of microfibrils exists in some tissues, with a supertwisted morphology comprising 5 molecules, with molecules belonging to one microfibril interdigitating with its neighbours [4]. The extent to which the molecules are tilted with respect to the fibril axis has been suggested to vary between tissues, with measurements of approximately 5° in large heterogeneous fibrils (typical of skeletal tissues such as tendon), and up to 17° in the thinner, uniform sized corneal fibrils [5,6] At larger hierarchical scales the stiffness of collagenous structures reduces, due to an increasing number of deformation mechanisms [7]. The primary deformation mechanism is dependent on the geometry of the tissue: for highly aligned tissues such as tendon and ligament, the relative sliding of fibrils dominates [8], while in tissues with more complex patterns of collagen arrangement such as cartilage and blood vessels, reorientation of the fibrillar architecture also plays a fundamental role [9,10].

The hierarchical deformation behaviour of collagen is a topic of significant current interest, and recent pioneering work has measured the mechanisms by which collagen confers mechanical toughness to skin [11] and tendon [8], the most dominant of which is interfibrillar

slippage. At a molecular scale, it has been suggested that the geometry of the tropocollagen molecule permits pulsed intermolecular slippage when the elastic limit of a fibril is reached [7], providing a further source of toughness. While these characteristics are vitally important in the function of organs that undergo large deformations, there has been little study of the hierarchical deformation mechanisms in tissues that undergo small deformations, such as the cornea. The collagen network in the cornea is unique, in that it confers both mechanical stability and transparency, the latter due to the regular spacing and size of collagen fibrils, which are arranged into approximately 240 flattened and highly aligned lamellae [12,13]. The cornea is the primary lens of the eye, and as such must maintain precisely its curvature in order to maintain clear vision. In health, the human cornea has been shown to deform little over physiological ranges of intraocular pressure (IOP) [14,15], however degenerative diseases such as keratoconus [16] and invasive surgical procedures [17–19] perturb the collagen network, leading to changes in corneal morphology that affect vision. While the anisotropic collagen network in cornea has been used to inform mechanical models [20–22], the deformation mechanisms of corneal collagen remain largely unknown. The regular fibrillar structure of corneal collagen (Figure 1) lends itself to X-ray diffraction (XRD) studies, which reveal information about the fibril spacing, diameter and orientation [23], measurements that cannot be obtained from other tissues, as well as molecular morphology and arrangement. The cornea therefore could be an ideal tissue for elucidating the fine structural response of collagenous tissues in general.

The healthy intact cornea deforms almost perfectly elastically under quasi-static pressure testing [24,25], suggesting there is little reorientation or interfibrillar/interlamellar sliding, which require significant energy expenditure [26]. The majority of deformation due to increases in IOP occur in the periphery [27] with the stiffer central and paracentral region [28,29] maintaining approximately the same shape. The lower stiffness of the periphery is likely associated with the transition in the arrangement of fibrils from predominantly radial to predominantly circumferential [30] meaning proportionally less collagen is recruited in the region during changes in IOP. The network of elastic tissue, that predominantly exists in the peripheral cornea [31], likely contributes to this elastic response, but it must be accompanied by an efficient collagenous deformation mechanism. This may be associated with the straightening of some hierarchical crimp [32], or of small deformations within the fibrils. This primary deformation mechanism needs to be elucidated in order to begin to understand the molecular basis for the dysfunction of the cornea.

The objective of this study is to elucidate the deformation mechanisms of corneal collagen at small applied strains. To achieve this, fresh human corneas were tested via quasi-static extensometry (tensile strip testing) and simultaneously imaged using small- (SAXS) or wide- (WAXS) angle X-ray scattering to elucidate the hierarchical deformation mechanisms of the collagen network. Extensometry was chosen as it is a simple, unambiguous test that is compatible with confined XRD stages and is easily analysed. Digital image correlation (DIC) was carried out to determine the local distribution of strain, and its relationship with local variations in the molecular and fibrillar architecture. Lastly, a scattering model was developed to quantify molecular tilt relative to the fibril axis.

Materials and Methods

Specimen preparation

In accordance with the tenets of the Declaration of Helsinki, a total of 17 post-mortem human donor cornea-scleral disks, aged between 21 and 90 years old, were obtained from UK eye banks. 9 corneas were assigned to a SAXS study and 8 to a WAXS study. The tissue was received following storage in culture media at a temperature of 37ºC for a period of 2 months. In order to reverse the tissue swelling that occurred during storage and return the

corneas to physiological hydration, the organ culture was supplemented with a 15% dextran solution for a period of 2 days prior to data collection.

Immediately prior to data collection, a 3.5 mm wide strip was cut along the vertical meridian of each cornea-scleral disk using a custom-made cutting device. The thickness of the corneal strip was recorded using an ultrasound pachymeter (DGH Pachmate 55; DGH Technologies, Exton, PA).

Extensometer

A custom-built extensometer comprising a piezo linear stage (Q-545-240, PI, driven by PIShift E-871 controller) and 4.9 N tension/compression load cell (Model 31, RDP) was used to apply static loads to the tensile strips. The stage and load cell were secured to fixed arms, which in turn were attached to removable serrated paddles, on to which the tensile specimen was carefully adhered using cyanoacrylate adhesive (Loctite). The stage and load cell were mounted on a bespoke base plate that included a large central hole to allow the beam to reach the entire specimen.

A preliminary experiment was carried out to ascertain the strains to be applied to the specimen. Synchrotron x-ray beamline time constraints limited the number of specimens and scans per specimen, so to adequately power the study 4 strain increments were applied. Increments were chosen that best covered the regions of interest on the nonlinear stress-strain curve [33], which includes features commonly known as the “toe” region, followed by a “heel” with increasing gradient, then a linear region that extends until failure. The tensile strain that gives rise to a stress equal to physiological hoop stress (10-20 kPa assuming physiological morphology [34]) was also measured. The preliminary study found the physiological stress to be reached at an average strain of 1.4%, the centre of the heel at 2.8% and the commencement of the linear region at 5%. A further strain of 8% was chosen for comparison with other extensometry studies, with higher strains rejected due to unreasonable relaxation times. A series of x-ray scattering patterns were obtained along the central axis of the specimen at each of these strain increments, and additionally at the initial tare preload, which was used to remove slack from the specimen.

X-ray scattering

Small-angle x-ray scattering [17] was carried out on Beamline I22 at Diamond Light Source (Didcot, UK), using an x-ray beam of wavelength 1 Å (12.4 keV), with an approximately elliptical profile with major axis parallel to the direction of stretch. The beam profile major and minor axial lengths at the specimen were approximately 300 μm and 150 μm. A Pilatus 2P3M photodetector (Dectris, Switzerland) collected scattered light at a distance of 6.8 m from the specimen, with the majority of the scatter path in an evacuated tube to reduce air scattering. This setup allowed examination of the fibrillar architecture of corneal collagen at length scales ranging from 10 nm to 100 nm. The 58.380 Å peak associated with the [001] crystal plane reflection of powdered silver behenate was used to centre and calibrate the images.

Wide-angle x-ray scattering (WAXS) was carried out on Beamline I02 at Diamond Light Source, using an x-ray beam of wavelength 0.979 Å (1.27 keV) and an elliptical beam profile of 50 μm × 90 μm. A Pilatus 3S6M photodetector (Dectris, Switzerland) collected scattered light at a distance of 0.3 m from the specimen. This setup allowed examination of the molecular arrangement of corneal collagen at length scales ranging from 0.2 nm to 2 nm. The 3.04 Å peak associated with the [104] reflection of calcium carbonate was used to centre and calibrate the images.

Example SAXS and WAXS images, and the associated radial scattering intensity profiles are shown in Figure 2. Features of interest at the fibrillar scale were the interfibrillar spacing, fibril diameter, D-period and the in-plane (polar) arrangement of fibrillar collagen. At the molecular scale the intermolecular spacing, collagen residue spacing and polar arrangement of molecules were of interest.

At each strain increment starting with the tare load, scatter patterns were obtained at 300 μm axial intervals close to the central axis of the strip (Figure 3A). Each pattern was obtained using a 1 second exposure, and between exposures the beam was blocked to minimise specimen dose. The total scan time at each strain increment was 90 seconds. Each strain increment was applied over 30 seconds, and then allowed to relax for (10, 15, 20, 30) minutes for (1.4%, 2.8%, 5%, 8%) strains. This was found to achieve approximately 80% of equilibrium stress relaxation in each case, and thereby ensuring no significant stress relaxation occurred during data collection. The specimens were sprayed with distilled water using a perfume atomizer at regular intervals to maintain specimen hydration. The hydration protocol was developed in a preliminary study that maintained specimen hydration to within a band of ±2%. Significant drying typically manifested in an increase in tensile force, which relaxed rapidly when the sample was sprayed. Samples that were found to dry excessively, defined as a drop in hydration of greater than 5%, were rejected from the study.

Digital image correlation

Fiducial paint markers were sprayed onto tensile strips prior to attachment to the extensometer**.** Spray paint (black and white, Valspar) was found to make no discernible difference to SAXS images, and the extra WAXS peaks did not overlap with any features of interest. The paint speckles optimised the DIC process and were discrete enough not to provide another surface layer to the specimens. It has been shown in a separate study that the addition of such a speckle pattern to specimens does affect their mechanical response [25].

In order to determine strain fields, photographs of the specimen were taken immediately after each WAXS line scan, by removing the extensometer from the primary stage and placing it under a dissection microscope. Acquired images were analysed using previously described custom software for semi-automatic digital image correlation and tracking [35]. This allowed the local strain field to be calculated reliably to a resolution of approximately 300 μm. The extensometer was sufficiently rigid that moving it did not perturb the specimen.

Scatter analysis

All analysis was carried out using bespoke software developed in-house in the Matlab (Mathworks) environment. Image centring and radial calibration were carried out using a brute-force algorithm that maximises the height of the circumferentially integrated calibration peak at every possible centre position. This proved to be accurate and reproducible to a resolution of approximately 0.01 pixels.

Before data images could be analysed the grid lines associated with the tiled nature of the detector were removed by filling their occupied space with pixel values from the symmetrically opposite side of the image. The image was centred such that no important peak fell on a grid line that could not be infilled by symmetry, and so no further image preparation was needed.

A detailed explanation of the analysis procedures for SAXS and WAXS of collagen can be found elsewhere [36,37] and is described briefly here. Images were converted to cylindrical polar form, with z representing pixel intensity, and data were split into two circumferential

populations: parallel (within ±45° of applied load in the positive and negative directions), and perpendicular (Figure 3B – 3C).

For WAXS, two exponential background subtractions were made to isolate the intermolecular and collagen residue spacing peaks. Gaussian fits were applied to both peaks. The angular dependence of the integrated intermolecular peak (Figure 3D) was used to calculate polar distributions of molecular orientation (Figure 3E). These distributions can be represented as polar patch plots (Figure 3E, insert).

For SAXS, exponential background subtractions were made to isolate the interfibrillar peak and the Bessel peaks associated with the cylinder scattering of the fibrils (see Figure 2C). Gaussian fits were applied to the reduced interfibrillar peak and meridionals 3, 5, 8, 9 and 12 to calculate accurately the average interfibrillar spacing and D-period, respectively. A Bessel function was fitted to calculate the average fibril diameter. The angular dependence of the integrated interfibrillar peak was used to calculate the angular distribution of fibrillar orientation at each scan position.

Scattering model

Polar orientation plots reflecting the angular distribution of tropocollagen molecules can be calculated readily from WAXS scatter images as discussed above. These plots are a convolution of the fibrillar orientation and the molecular tilt relative to the fibril axis (see Figure 1). To determine changes in molecular tilt associated with strain, a scattering model was written based upon the assumption that tropocollagen molecules can be represented as helices with axis parallel to the respective fibril (an approximation of the geometry suggested in (4)). This model uses an approach described in detail in [38]. A brief summary follows.

Assuming that at each position on the fibril adjacent molecules are parallel to one-another, the scatter pattern from such a fibril can be approximated as a sum of the scatter patterns from an arrangement of straight lines at a tilt relative to the fibril axis equal to the helical tilt (illustrated in Results). Ignoring intramolecular scattering features, a straight molecule can be approximated as a line of finite spheres. The structure factor of a sphere is

$$f(S) = \frac{2\pi RS\cos(2\pi RS) - \sin(2\pi RS)}{4\pi^2 R^3}$$

where *S* is the magnitude of the scattering vector and R is the radius of the sphere. The structure factor associated with an arrangement of N spheres is

$$F(\boldsymbol{S}) = \sum_{n=1}^{N} f(S) e^{2\pi i \boldsymbol{S}\cdot\boldsymbol{a}_n}$$

where $\mathbf{a}_n$ is the position vector of the n^{th} sphere. The scattered intensity, as measured with a detector, is

$$I(\boldsymbol{S}) = F(\boldsymbol{S})F^*(\boldsymbol{S})$$

and to construct a scatter image **S** is varied to correspond with scattering to each pixel of the image. The model comprised 97 lines of 400 spheres. Each sphere was 0.05 Å in diameter, and separated by 0.1 Å. The lines were arranged in a hexagonal lattice with nearest neighbour spacing 1.9 Å, and corresponding Bragg spacing 1.71 Å [39]. Corneal WAXS patterns show only one discernible peak associated with the intermolecular spacing, indicating that the coherence length is small. To reflect this in the model, a preliminary experiment was carried out to determine the extent of disorder required to produce a single

peak of correct width, and it was found that randomly displacing each line by up to 0.6 Å in *x* and *y* yielded the closest match. It should be noted that the packing arrangement of collagen molecules is still not clear [6], however for the purpose of determining molecular tilt from comparison of SAXS and WAXS patterns, the lattice arrangement had little effect. To produce a scatter image for a single fibril with a particular molecular tilt, the line model was run 180 times at 2° azimuthal increments, with lines tilted at the requisite inclination angle. The resulting image was then convoluted with fibril orientation data in central cornea from SAXS experiments to produce a modelled WAXS image. The modelled molecular orientation distributions at varying pitch were compared with those observed experimentally using a least squares fit.

Results

Changes in Collagen Structure

A graphical overview of the X-ray scattering results is shown in Figure 4. When averaged over all fibril orientations, the D-period appeared to be unaffected by changes in strain. However, measurement of the same parameter in just the fibrils aligned parallel to the direction applied strain, revealed a significant increase in D–periodicity between 2.8% and 8% applied strain ($p<0.001$), implying fibril elongation. In the orthogonal direction the mean D-period dropped significantly ($p<0.001$) following the 1.4% strain increment, implying fibril shortening, and remained relatively unchanged thereafter.

Fibril diameter, measured only as an overall average due to limited signal, showed a negative trend with strain that was significant at the 2.8% and 5% increments ($p<0.05$). As strain increased the Bessel function fit became poorer, suggesting the fibrils were increasingly variable in diameter, losing their cylindrical shape, or coming into contact with one another.

Although statistically insignificant, the spacing between fibrils appeared to increase slightly as a function of strain, whilst the inter-fibrillar coherence, which provides a measure of crystallinity [40,41], decreased significantly at strains of 2.8% and above ($p<0.001$). The intermolecular spacing showed the converse, with collagen molecules aligned parallel to the direction of strain moving closer towards each other as strain increased ($p<0.05$), but showing little change in intermolecular coherence. It was noted in all experiments that despite maintaining hydration the specimens became more opaque with increased tensile strain.

An example of the normalised polar arrangement of collagen fibrils along the length of a representative specimen, and the variation associated with strain, is shown in Figure 5A. The equivalent plot for molecular orientation is shown in Figure 5B. Both fibrillar and molecular reorientation was evident from the smallest strain increment, although the most pronounced changes occurred between the 2.8% and 5% strain increments. At 8% applied strain the interfibrillar peak became much weaker and broader, making the fibril orientation plot more sensitive to noise. At all strains, the molecular distributions were more isotropic than their fibrillar counterparts, supporting the hypothesis that molecules are tilted relative to the fibril axis.

Local Strain Effects

The distribution of tensile strain was found to be non-uniform along the length of each specimen. Although maximal deformation occurred in the peripheral cornea, the central ~2 mm of the cornea was found to exhibit greater deformation than the adjacent paracentral region. Figure 6A shows the local strain field in a representative specimen at 5% applied

strain, with the corresponding distributions of longitudinal and orthogonal strain along the centre of the strip shown in Figure 6B. The perpendicular strain was between 2 and 3 times that in the longitudinal direction, and is clearly non-uniform as evidenced by the formation of longitudinal creases. The anisotropic arrangement of collagen molecules at 5% applied strain is shown in Figure 6C, and the variation in anisotropy (defined as ratio of peak parallel signal to peak perpendicular signal) with length at all strains is shown in Figure 6D. This shows that reorientation as a mechanism for distributing local strain only becomes significant above 2.8% applied strain, and therefore at smaller strains another mechanism must dominate. The pattern of reorientation with strain correlated with the distribution of orthogonal strain and approximately with distance from the fixed ends, although in all specimens and all strains the central 3-4 mm showed even extents of reorientation.

Scatter Model

WAXS scatter patterns are a convolution of the fibrillar orientation and the molecular tilt relative to the fibril axis (Figure 1). The disordered hexagonal lattice arrangement of molecules is shown in Figure 7A. Assuming that tropocollagen molecules can be represented as helices with axes parallel to their respective fibril, the sum of several line models of fixed inclination and varying azimuth can simulate the helical arrangement of collagen molecules in a single fibril, as shown in Figures 7B and 7C. A modelled WAXS pattern for a single fibril with a molecular tilt of 16° is shown in Figure 7D. The convolution of this modelled WAXS pattern with experimental fibril orientation data (obtained using SAXS), produced the modelled WAXS pattern showed in Figure 7E. The distribution of x-ray scatter intensity in the modelled WAXS pattern (Fig 7E) is in close accord with the experimentally obtained WAXS pattern from the cornea at the tare load (Fig 7F).

Using the average experimentally measured polar distribution of molecules aligned in the parallel direction range as a fitting parameter, it was possible to use the model to find the corresponding average molecular tilt at each strain increment. Figures 7G and 7H show averaged experimentally obtained fibrillar and molecular orientation distributions and the corresponding molecular model at the tare load and 5%, respectively. To a tolerance of 1°, the average tilts are shown in Table 1. The significant drop in molecular tilt may be indicative of a subfibrillar strain mechanism, in that the molecules appear to be stretching like coiled springs. It was not possible to use this approach to calculate tilt at 8% applied strain due to irregularities in the polar arrangement of both fibrils and molecules.

Discussion

The molecular and fibrillar architecture of corneal collagen has been examined under load. The fibrillar arrangement in the tare loaded state revealed preferential orientation in the superior-inferior and nasal-temporal directions in the central and paracentral cornea, changing to a circumferential preference through the periphery and into the limbus, which is in line with previous reports of unloaded human cornea [30]. Straining the tissue by as little as 1.4% perturbed the arrangement at both the molecular and fibrillar scale. The most pronounced change was in the crystallinity of the fibril network, which probably explains the increased opacity of the tissue. While the interfibrillar spacing was found to vary considerably under strain, the average value did not change significantly, with the results indicating a weak positive trend. Auxetic behaviour (negative Poisson's ratio) at the fibrillar scale under tensile strain has been reported in cornea previously at much higher strain and attributed to the proteoglycan network maintaining a minimum interfibrillar distance [42], and our findings would appear to support this. At the macroscopic scale, DIC measurements showed that the specimen behaved like a typical biological material, with a high Poisson's ratio (greater than 1) and longitudinal creases that presumably took up all the orthogonal strain. High Poisson's ratios are common in soft tissue in tension, and have been reported, for instance, in articular cartilage [43]. The intermolecular strain mirrors the strain in the fibril

diameter, as would be expected, suggesting there is no volumetric change below the molecular scale. Comparison of volumetric changes at the molecular and fibrillar scale suggests a small load-induced flow of water from the intrafibrillar to the interfibrillar compartment.

The applied deformations manifest themselves at several hierarchical scales, which are illustrated in Figure 8. Firstly the application of the tare load straightens the specimen (Figure 8A) and applies a small strain differential across the thickness [44]. Lamella inclination angle ranges have been measured using second harmonic generation microscopy (SHG) following pressure fixation and found to average approximately 12° [45]. While much of the angle is likely to be associated with lamellar interweaving, some may be associated with residual crimp (Figure 8B). Analysis by Grytz and Meschke on the extensibility of crimped tissue [46] would suggest any residual crimp would be taken up by the first strain increment. The magnitude of lamellar crimp *in vivo* is still not fully understood, and the majority of the spread in inclination angle is likely not to be crimp and instead associated with intertwining of adjacent lamellae. The linear trends in fibril strain (from D-period measurements) and changes in molecular tilt measured in this study over the 0% to 2.8% increments would suggest that if any lamella-scale crimp does persist past the tare load, it is not a significant deformation mechanism. Corneal fibrillar crimp (Figure 8C) has been reported in SHG [47] and TEM [48] studies, the latter of which showed residual crimp following an applied tensile strain of 10%. In this study the polar arrangement of fibrillar collagen was found to change significantly at the 2.8% strain increment and above, but given that the fibrillar scatter from all lamellae contribute equally to the scatter pattern it is not possible to separate crimp straightening with reorientation of lamellae (Figure 8D). Evidence of lamella reorientation comes from the changes in the measured ratio of parallel to perpendicular fibril scatter, as without large-scale reorientation fibrils aligned close to perpendicular should not be significantly perturbed by the applied strain. Clearly lamella reorientation is an artefact of extensometry, in that fibrils that are cut at the edges of the excised strip are released of tension, causing the specimen to narrow in the middle. Preliminary studies not shown in this report found anomalous arrangements of collagen in the region within 600 μm of a cut edge, but outside that region the arrangement was uniform across the width of the specimen. The cut edge of specimens was still well-defined at the end of the experimental protocol, meaning that cut fibril slippage is an unlikely mechanism for lamella reorientation. It is likely, then, that lamella reorientation is caused by a combination of macroscopic geometry changes (the applied strain and the orthogonal contraction), as well as the straightening of intertwined lamellae.

The straightening of molecular tilt relative to the fibril axis (Figure 8E) has not been reported before and may be an important deformation mechanism in collagen. It has been suggested that collagen fibrils fall into two types: [49] the T-type (found for example in tendon) being heterogeneous in diameter, with a small molecular tilt (<5°) and exhibiting significant crimp when unloaded; and the C-type, native to the cornea and other tissues such as cartilage and skin, which are uniform in diameter and molecular tilt (17°), and are significantly more flexible than T-type fibrils [50]. The calculated tilt of 16° for tare loaded specimens supports the hypothesis that the spread of molecular orientation about the fibrillar arrangement is due to the helical tilt of molecules. Continuing with the helical approximation, the observed changes in molecular tilt at strain increments (1.4%, 2.8%, 5%) would suggest the fibrils are deforming by an average of (0.9%, 1.8%, 2.1%). Given that the tilts were calculated for fibrils oriented within a range ±45° about the direction of applied strain, it is possible that the significant majority of the deformation in parallel-aligned collagen is taken up by molecular straightening up to the 2.8% increment, with other mechanisms being invoked beyond that. A problem with this interpretation is that the D-period is intrinsically linked with molecular tilt α via the relation $\cos\alpha = {}^{D_c}/_{D}$ where D_c is the measured corneal D-period and D is the molecular stagger [51]. The measurements of D-period in this study do not obey this relation,

as at 5% applied strain, and 11° tilt the measured D-period change in the parallel direction should be 2.1% rather than 0.6%. This discrepancy may be an artefact of using meridional peak positions in the calculation of the D-period rather than spread or range, as it was noted qualitatively that the peaks became increasingly asymmetric as strain increased.

In accordance with previous work involving inflation testing, [18,27] , the peripheral cornea was found to deform more than the medial regions. It is possible that such a mechanism prevents changes in intraocular pressure from significantly affecting focus. The recent discovery of an elastic sheet-like network in the periphery [31,52] has strengthened suggestions that the peripheral cornea acts as a strain absorber, deforming under changes in intraocular pressure and thereby minimising changes in curvature in the paracentral and central cornea [29], which could be detrimental to vision. Such a system would function best if the deformation was as efficient as possible, and a synergy between networks of near-lossless elastic fibres and collagen fibrils that can deform longitudinally via a subfibrillar mechanism may be the optimal arrangement. Longitudinal fibril deformation will also limit changes in lateral packing that could have an adverse effect on corneal transparency. The increased strain in the central cornea compared with the paracentral region has been reported before under inflation testing [34], and was associated with increased membrane stress (due to variations in curvature). It is possible that geometry also explains this result, as under the tare load orthogonal creases were evident in the central cornea, which were presumably due to the straightening of a normally curved structure [44], giving rise to internal stress. The fact that the D-period drops by a significant amount (decreasing from 65.1 nm to 64.9 nm) in the orthogonal direction under load would suggest the collagen network is under significant internal stress in vivo which is likely to be associated with the swelling pressure of the hydrated glycosaminoglycan network. The orthogonal D-period does not change significantly beyond the initial 1.4% strain increment, which corresponds to an average orthogonal strain of 1.1%. Assuming the decreased D-period is derived from collagen released of all internal stress, corneal internal pressure could be derived from consideration of the stress-strain behaviour of corneal collagen fibrils.

Keratoconus is regarded as a degenerative disease affecting the corneal collagen network, in which a degeneration of the fibrillar structure and an increased propensity of fibrils to slide relative to one-another gives rise to altered macroscopic morphology and astigmatism [16]. It is possible that in this study some fibril sliding occurred at the higher strain increments, as the changes in the polar distribution of parallel fibrils (reflecting straightening of crimp or reorientation of lamellae), combined with the elongation of fibrils measured via molecular tilt calculations, does not account for the magnitude of the applied strain. To determine the magnitude of sliding, an approach that incorporates light microscopy, such as previous studies on tendon [8] and intervertebral disc annulus [53] could be utilized. It is likely that a combined approach of mechanical stimulus and X-ray scattering, such as that presented here, on keratoconus corneas could yield valuable information about changes in hierarchical mechanical properties of diseased tissue. This approach may also have utility in determining differences in the micromechanical properties of healed/scarred tissue following invasive surgery [54,55], or tissue treated using crosslinking techniques [56].

Many of the techniques demonstrated in this study are transferable to other tissues. Measurement of the orientation of fibrils is possible by quantifying the azimuthal distribution of signal in the meridional peaks, which are ubiquitous to all collagenous tissue, while the intermolecular spacing peak features in all tissues, and provides a measurement of molecular orientation. Comparison of fibrillar and molecular orientation via the modelling approach shown in this work then provides a measure of molecular tilt relative to the fibril axis. This has the potential to be a powerful tool, as the change in molecular tilt is related to the stress within the fibril. Changes in the tilt response of tissue under known loads in, for instance, degenerative diseases such as osteoarthritis, or fibrosis associated with vascular disease, is indicative of a change in the fibrillar mechanical environment. Such changes

could be quantified to enhance the accuracy of models of disease. Furthermore, the findings presented in this study could be incorporated into the design of collagen-based artificial corneas that are being developed to address world-wide shortages of corneal donor tissue, and other regenerative medicine applications involving connective tissues [57].

Acknowledgements

This work was funded by a Programme Grant MR/K000837/1 from the Medical Research Council (to KMM). We thank the NHSBT for supply of human corneas. We also thank the following staff from Diamond Light Source for the development of control software and scripting: Chris Sharp, James O'Hea, Peter Holloway and Ronaldo Mercado.

References

[1] N. Sasaki, S. Odajima, Stress-strain curve and Young's modulus of a collagen molecule as determined by the X-ray diffraction technique, J. Biomech. 29 (1996) 655–658.

[2] P. Bruckner, Suprastructures of extracellular matrices: paradigms of functions controlled by aggregates rather than molecules, Cell Tissue Res. 339 (2010) 7–18.

[3] K.E. Kadler, C. Baldock, J. Bella, R.P. Boot-Handford, Collagens at a glance, J. Cell Sci. 120 (2007) 1955–1958.

[4] J.P.R.O. Orgel, T.C. Irving, A. Miller, T.J. Wess, Microfibrillar structure of type I collagen in situ, Proc. Natl. Acad. Sci. 103 (2006) 9001–9005.

[5] D.F. Holmes, C.J. Gilpin, C. Baldock, U. Ziese, A.J. Koster, K.E. Kadler, Corneal collagen fibril structure in three dimensions: Structural insights into fibril assembly, mechanical properties, and tissue organization, Proc. Natl. Acad. Sci. 98 (2001) 7307–7312.

[6] V. Ottani, D. Martini, M. Franchi, A. Ruggeri, M. Raspanti, Hierarchical structures in fibrillar collagens, Micron. 33 (2002) 587–596.

[7] M.J. Buehler, Nature designs tough collagen: explaining the nanostructure of collagen fibrils, Proc. Natl. Acad. Sci. 103 (2006) 12285–12290.

[8] H.S. Gupta, J. Seto, S. Krauss, P. Boesecke, H.R.C. Screen, In situ multi-level analysis of viscoelastic deformation mechanisms in tendon collagen, J. Struct. Biol. 169 (2010) 183–191.

[9] Y. Sasazaki, R. Shore, B.B. Seedhom, Deformation and failure of cartilage in the tensile mode, J. Anat. 208 (2006) 681–694..

[10] J.S. Bell, A.O. Adio, A. Pitt, L. Hayman, C.E. Thorn, A.C. Shore, J.L. Whatmore, C.P. Winlove, Microstructure and mechanics of human resistance arteries, Am. J. Physiol. Circ. Physiol. 311 (2016) H1560–H1568.

[11] W. Yang, V.R. Sherman, B. Gludovatz, E. Schaible, P. Stewart, R.O. Ritchie, M.A. Meyers, On the tear resistance of skin, Nat. Commun. 6 (2015).

[12] J.P.G. Bergmanson, J. Horne, M.J. Doughty, M. Garcia, M. Gondo, Assessment of the number of lamellae in the central region of the normal human corneal stroma at the resolution of the transmission electron microscope, Eye Contact Lens. 31 (2005) 281–287.

[13] K.M. Meek, C. Knupp, Corneal structure and transparency, Prog. Retin. Eye Res. 49 (2015) 1–16.

[14] M. Asejczyk-Widlicka, B.K. Pierscionek, The elasticity and rigidity of the outer coats of the eye, Br. J. Ophthalmol. 92 (2008) 1415–1418.

[15] B. Jue, D.M. Maurice, The mechanical properties of the rabbit and human cornea, J. Biomech. 19 (1986) 847–853.

[16] M. Koster, C. Boote, K. Meek, P. Fowler, C. Girkin, G. Meschke, R. Grytz, Inter-and intra-lamellar slippage of collagen fibrils as a potential mechanism of keratoconus progression, Invest. Ophthalmol. Vis. Sci. 54 (2013) 1642.

[17] M.K. Smolek, Holographic interferometry of intact and radially incised human eye-bank corneas, J. Cataract Refract. Surg. 20 (1994) 277–286.

[18] P.D. Jaycock, L. Lobo, J. Ibrahim, J. Tyrer, J. Marshall, Interferometric technique to measure biomechanical changes in the cornea induced by refractive surgery, J. Cataract Refract. Surg. 31 (2005) 175–184.

[19] E. Borasio, J.S. Mehta, V. Maurino, Torque and flattening effects of clear corneal temporal and on-axis incisions for phacoemulsification, J. Cataract Refract. Surg. 32 (2006) 2030–2038.

[20] P.M. Pinsky, D. van der Heide, D. Chernyak, Computational modeling of mechanical

anisotropy in the cornea and sclera, J. Cataract Refract. Surg. 31 (2005) 136–145.
[21] H. Studer, X. Larrea, H. Riedwyl, P. Büchler, Biomechanical model of human cornea based on stromal microstructure, J. Biomech. 43 (2010) 836–842.
[22] C. Whitford, H. Studer, C. Boote, K.M. Meek, A. Elsheikh, Biomechanical model of the human cornea: Considering shear stiffness and regional variation of collagen anisotropy and density, J. Mech. Behav. Biomed. Mater. 42 (2015) 76–87.
[23] K.M. Meek, A.J. Quantock, The use of X-ray scattering techniques to determine corneal ultrastructure, Prog. Retin. Eye Res. 20 (2001) 95–137.
[24] T.K. Tonge, B.J. Murienne, B. Coudrillier, S. Alexander, W. Rothkopf, T.D. Nguyen, Minimal preconditioning effects observed for inflation tests of planar tissues, J. Biomech. Eng. 135 (2013) 114502.
[25] C. Whitford, A. Joda, S. Jones, F. Bao, P. Rama, A. Elsheikh, Ex vivo testing of intact eye globes under inflation conditions to determine regional variation of mechanical stiffness, Eye Vis. 3 (2016) 21.
[26] C.T. Thorpe, C. Klemt, G.P. Riley, H.L. Birch, P.D. Clegg, H.R.C. Screen, Helical sub-structures in energy-storing tendons provide a possible mechanism for efficient energy storage and return, Acta Biomater. 9 (2013) 7948–7956.
[27] B.L. Boyce, J.M. Grazier, R.E. Jones, T.D. Nguyen, Full-field deformation of bovine cornea under constrained inflation conditions, Biomaterials. 29 (2008) 3896–3904.
[28] S.-Y. Woo, A.S. Kobayashi, W.A. Schlegel, C. Lawrence, Nonlinear material properties of intact cornea and sclera, Exp. Eye Res. 14 (1972) 29–39.
[29] A. Elsheikh, C.W. McMonnies, C. Whitford, G.C. Boneham, In vivo study of corneal responses to increased intraocular pressure loading, Eye Vis. 2 (2015) 20.
[30] H. Aghamohammadzadeh, R.H. Newton, K.M. Meek, X-ray scattering used to map the preferred collagen orientation in the human cornea and limbus, Structure. 12 (2004) 249–256.
[31] P.N. Lewis, T.L. White, R.D. Young, J.S. Bell, C.P. Winlove, K.M. Meek, Three-dimensional arrangement of elastic fibers in the human corneal stroma, Exp. Eye Res. 146 (2016) 43–53.
[32] M. Comninou, I.V. Yannas, Dependence of stress-strain nonlinearity of connective tissues on the geometry of collagen fibres, J. Biomech. 9 (1976) 427–433.
[33] Y.C.B. Fung, Elasticity of Soft Tissues in Simple Elongation, Am. J. Physiol. 213 (1967) 1532-. %3CGo.
[34] J.Ø. Hjortdal, Regional elastic performance of the human cornea, J. Biomech. 29 (1996) 931–942.
[35] C. Vergari, J. Mansfield, J.R. Meakin, P.C. Winlove, Lamellar and fibre bundle mechanics of the annulus fibrosus in bovine intervertebral disc, Acta Biomater. 37 (2016) 14–20.
[36] K.M. Meek, C. Boote, The use of X-ray scattering techniques to quantify the orientation and distribution of collagen in the corneal stroma, Prog. Retin. Eye Res. 28 (2009) 369–392.
[37] A. Abass, J.S. Bell, M.T. Spang, S. Hayes, K.M. Meek, C. Boote, SAXS4COLL: an integrated software tool for analysing fibrous collagen-based tissues, J. Appl. Crystallogr. In press.
[38] C.R. Cantor, P.R. Schimmel, Biophysical chemistry, part. II Techniques for the study of biological structure and function. WH Freeman and Co., Oxford, 1980.
[39] A. Maroudas, E. Wachtel, G. Grushko, E.P. Katz, P. Weinberg, The Effect of Osmotic and Mechanical Pressures on Water Partitioning in Articular-Cartilage, Biochim. Biophys. Acta. 1073 (1991) 285–294.
[40] J.W. Regini, G.F. Elliott, S.A. Hodson, The ordering of corneal collagen fibrils with increasing ionic strength, J. Mol. Biol. 336 (2004) 179–186.
[41] A.R. Stokes, The theory of X-ray fibre diagrams, Prog. Biophys. Biophys. Chem. 5 (1955).
[42] K. Patten, T. Wess, Suprafibrillar structures of collagen, evidence for local organization and auxetic behaviour in architectures, J. Biophys. Chem. 4 (2013) 103-109.
[43] D.M. Elliott, D.A. Narmoneva, L.A. Setton, Direct measurement of the Poisson's ratio of human patella cartilage in tension, Trans. Soc. Mech. Eng. J. Biomech. Eng. 124 (2002) 223–228.
[44] A. Elsheikh, K. Anderson, Comparative study of corneal strip extensometry and inflation tests., J. R. Soc. Interface. 2 (2005) 177–185.
[45] M. Winkler, G. Shoa, Y. Xie, S.J. Petsche, P.M. Pinsky, T. Juhasz, D.J. Brown, J. V Jester, Three-dimensional distribution of transverse collagen fibers in the anterior human corneal stromacorneal collagen fiber angle quantification, Invest. Ophthalmol. Vis. Sci. 54 (2013) 7293–7301.
[46] R. Grytz, G. Meschke, A computational remodeling approach to predict the physiological architecture of the collagen fibril network in corneo-scleral shells, Biomech. Model. Mechanobiol. 9 (2010) 225–235.

[47] Y. Mega, M. Robitaille, R. Zareian, J. McLean, J. Ruberti, C. DiMarzio, Quantification of lamellar orientation in corneal collagen using second harmonic generation images, Opt. Lett. 37 (2012) 3312–3314.
[48] X. Liu, L. Wang, J. Ji, W. Yao, W. Wei, J. Fan, S. Joshi, D. Li, Y. Fan, A Mechanical Model of the Cornea Considering the Crimping Morphology of Collagen FibrilsCrimping Morphology of Collagen Fibrils, Invest. Ophthalmol. Vis. Sci. 55 (2014) 2739–2746.
[49] V. Ottani, M. Raspanti, A. Ruggeri, Collagen structure and functional implications, Micron. 32 (2001) 251–260.
[50] F.H. Silver, I. Horvath, D.J. Foran, Mechanical implications of the domain structure of fiber-forming collagens: comparison of the molecular and fibrillar flexibilities of the α1-chains found in types I–III collagen, J. Theor. Biol. 216 (2002) 243–254.
[51] M. Marchini, M. Morocutti, A. Ruggeri, M.H.J. Koch, A. Bigi, N. Roveri, Differences in the fibril structure of corneal and tendon collagen. An electron microscopy and X-ray diffraction investigation, Connect. Tissue Res. 15 (1986) 269–281.
[52] T.L. White, P.N. Lewis, R.D. Young, K. Kitazawa, T. Inatomi, S. Kinoshita, K.M. Meek, Elastic microfibril distribution in the cornea: Differences between normal and keratoconic stroma, Exp. Eye Res. 159 (2017) 40–48.
[53] C. Vergari, D. Chan, A. Clarke, J.C. Mansfield, J.R. Meakin, P.C. Winlove, Bovine and degenerated human annulus fibrosus: a microstructural and micromechanical comparison, Biomech. Model. Mechanobiol. (2017) 1–10.
[54] C. Tamburrelli, A. Giudiceandrea, A.S. Vaiano, C.G. Caputo, F. Gulla, T. Salgarello, Underestimate of tonometric readings after photorefractive keratectomy increases at higher intraocular pressure levels, Invest. Ophthalmol. Vis. Sci. 46 (2005) 3208–3213.
[55] W.J. Dupps, S.E. Wilson, Biomechanics and wound healing in the cornea, Exp. Eye Res. 83 (2006) 709–720.
[56] K.M. Meek, S. Hayes, Corneal cross-linking–a review, Ophthalmic Physiol. Opt. 33 (2013) 78–93.
[57] S. Hayes, P. Lewis, M.M. Islam, J. Doutch, T. Sorensen, T. White, M. Griffith, K.M. Meek, The structural and optical properties of type III human collagen biosynthetic corneal substitutes, Acta Biomater. 25 (2015) 121–130.

Figure Captions

Figure 1. Hierarchical arrangement of collagen in the cornea. Abbreviations: MF – microfibril; TC – tropocollagen molecule. (TEM image courtesy of Nada Aldahlawi, unpublished work).

Figure 2. Illustrations of X-ray diffraction images and peak analysis. A. Example SAXS scatter pattern. B. Example WAXS scatter pattern. C Radial SAXS plot corresponding to panel A. D. Radial WAXS plot corresponding to panel B. Labelled peaks: Interfibrillar spacing (IF); Meridionals 3 and 5 (M3, M5); Bessel-function shaped fibril cylinder transform (used to measure fibril diameter) (B); Intermolecular spacing (IM). Dotted and dashed lines correspond to exponential background subtractions.

Figure 3. Illustrations of the experiment and analysis protocols. A. Schematic of the extensometry experiment with scan positions overlaid on the strip. B. Example SAXS pattern showing regions defined as parallel and perpendicular to the applied strain, for axial scattering (the regions are swapped for lateral scattering). C. Corresponding radial intensity plot for B, showing meridional peaks 3-8 as an example. D Example WAXS pattern with overlaid calculation for polar dependence of intermolecular peak. E. The azimuthal distribution of signal in the intermolecular peak in panel D reveals the polar distribution of molecules (after reflection-based removal of gridline). The process is the same for calculating the fibril distribution from SAXS images. Insert: Polar patch plot of the molecular distribution shown in panel E, used for compactness when showing multiple distributions across a specimen.

Figure 4. Averaged change in XRD metrics associated with strain. Error bars show SEM and are offset in x to avoid overlap. Parallel and perpendicular fibril diameters could not be ascertained due to loss of peak shape when strained.

Figure 5. Representative polar patch plots of collagen fibril orientation calculated from the interfibrillar peak distribution observed using SAXS (A) and the intermolecular peak distribution observed using WAXS (B), for representative specimens at varying strain. The anisotropy value is the ratio of maximum parallel collagen to maximum orthogonal collagen. Some SAXS plots are noisy or omitted due to loss in signal associated with disorder at the fibrillar hierarchy.

Figure 6. Distribution of local strain and associated reorientation for a representative tensile strip. x-axes of plots coincide. A. Original image of the tensile strip at 5% applied strain with local longitudinal strain field obtained using DIC overlaid. B. Average parallel and perpendicular strain along the centre of the strip. C. Polar patch plots of local collagen molecule orientation at 5% applied strain. D. Anisotropy measured as ratio of peak longitudinal to peak orthogonal orientation, for each strain increment.

Figure 7. Molecular model geometry and results. A. Axial view of representative line/filament arrangement, which is a disordered hexagonal lattice. B. Illustration of how a helical molecular arrangement (blue) relative to the fibril axis (black) is modelled by a sum of straight line geometries of varying inclination. C. Side view of line model geometry, with molecular tilt shown as inclination angle θ. For each value of θ, 180 scatter patterns were calculated at 2° azimuthal increments to simulate an arrangement of parallel helices. D. Scatter pattern from the disordered helix model with a tilt of 16°. E. Modelled scatter pattern from a helical model with tilt 16°, convoluted with the average fibril distribution at the tare load. F. Representative WAXS pattern from a specimen under the tare load. G. Averaged polar arrangement of fibrils (blue), molecules (red) and modelled molecules at a 16° tilt (black) for a specimen under the tare load. F. Polar arrangements for a specimen at 5% applied strain, with a fitted 11° tilt.

Figure 8. Average quasi-equilibrium tensile stress associated with each strain increment, with spans indicating ranges of strain over which illustrated deformation mechanisms may apply. A. Straightening of corneal curvature, occurs during application of tare load (millimetres). B. Lamellar crimp, arguable contribution at low strains based upon literature evidence (100s of microns). C. Fibrillar crimp measured using SAXS (100s of nanometres). D. Lamellar and fibrillar reorientation measured using SAXS (100s of nanometres). E. Straightening of molecular helical tilt relative to fibril axis measured using SAXS and WAXS (Angstroms).

Tables

Table 1: Molecular tilt at varying strain

Applied Strain	Average molecular tilt with respect to fibril axis
Tare	16°
1.4%	14°
2.8%	12°
5%	11°

Figure 1

Click here to download high resolution image

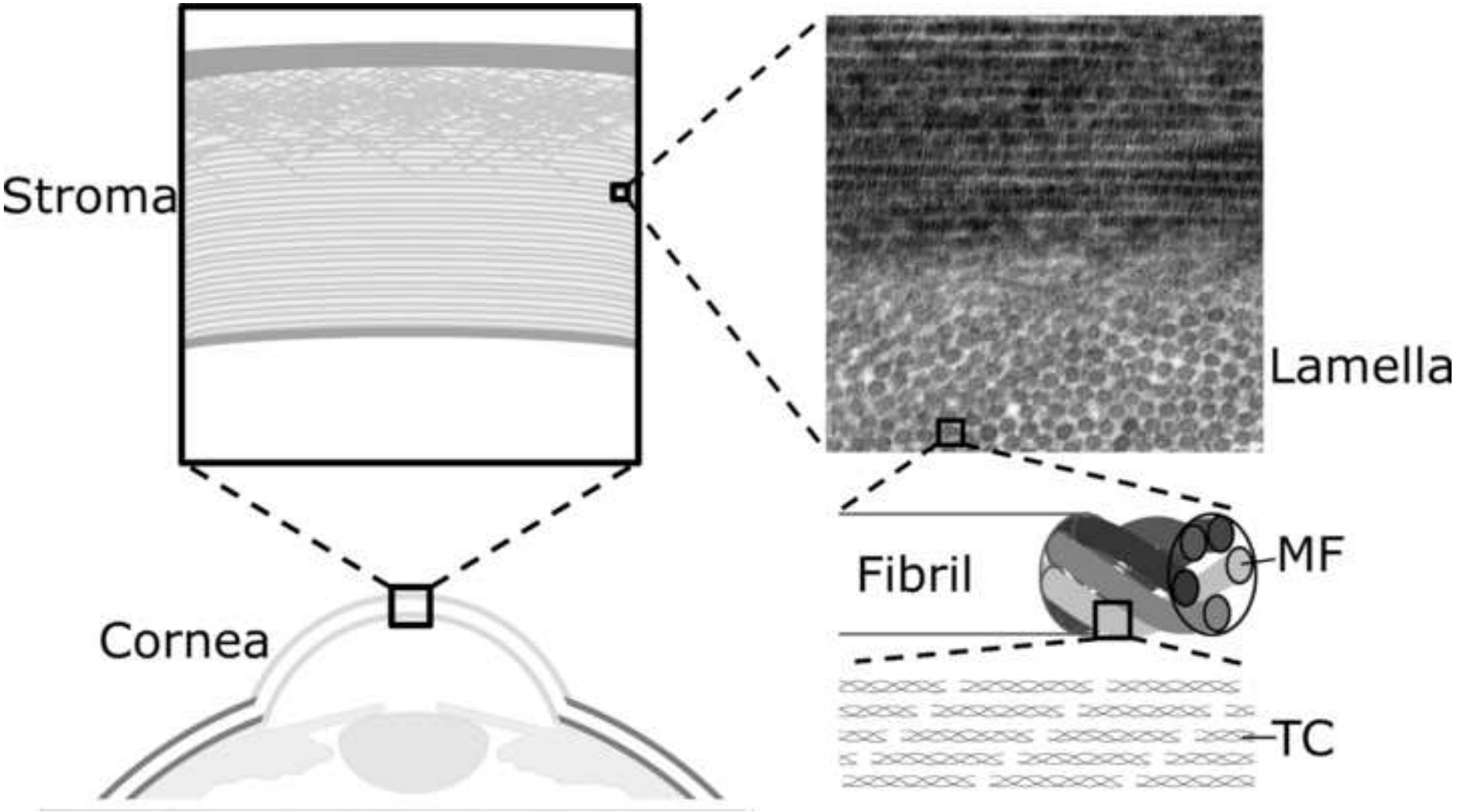

Figure 2

Click here to download high resolution image

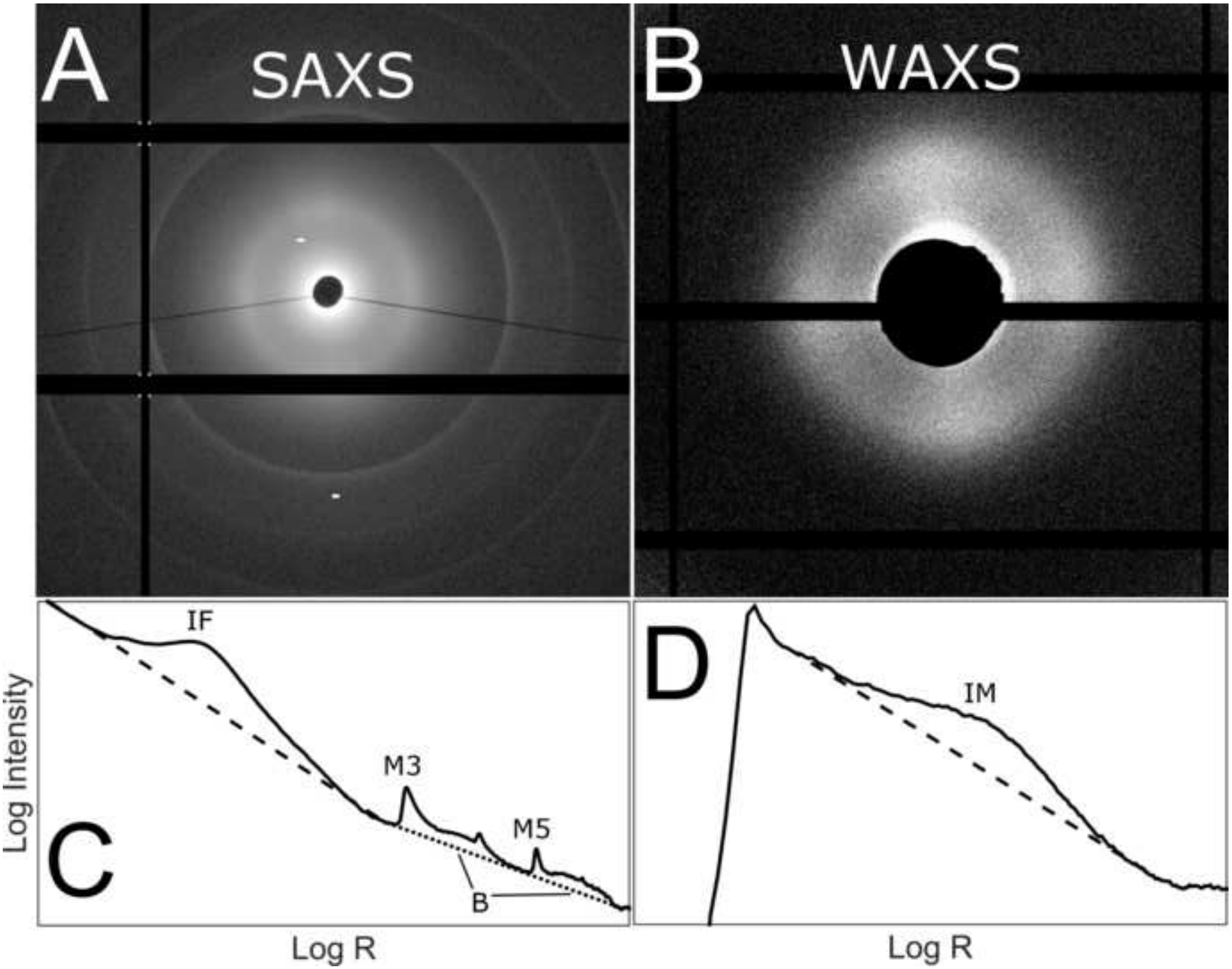

Figure 3

Click here to download high resolution image

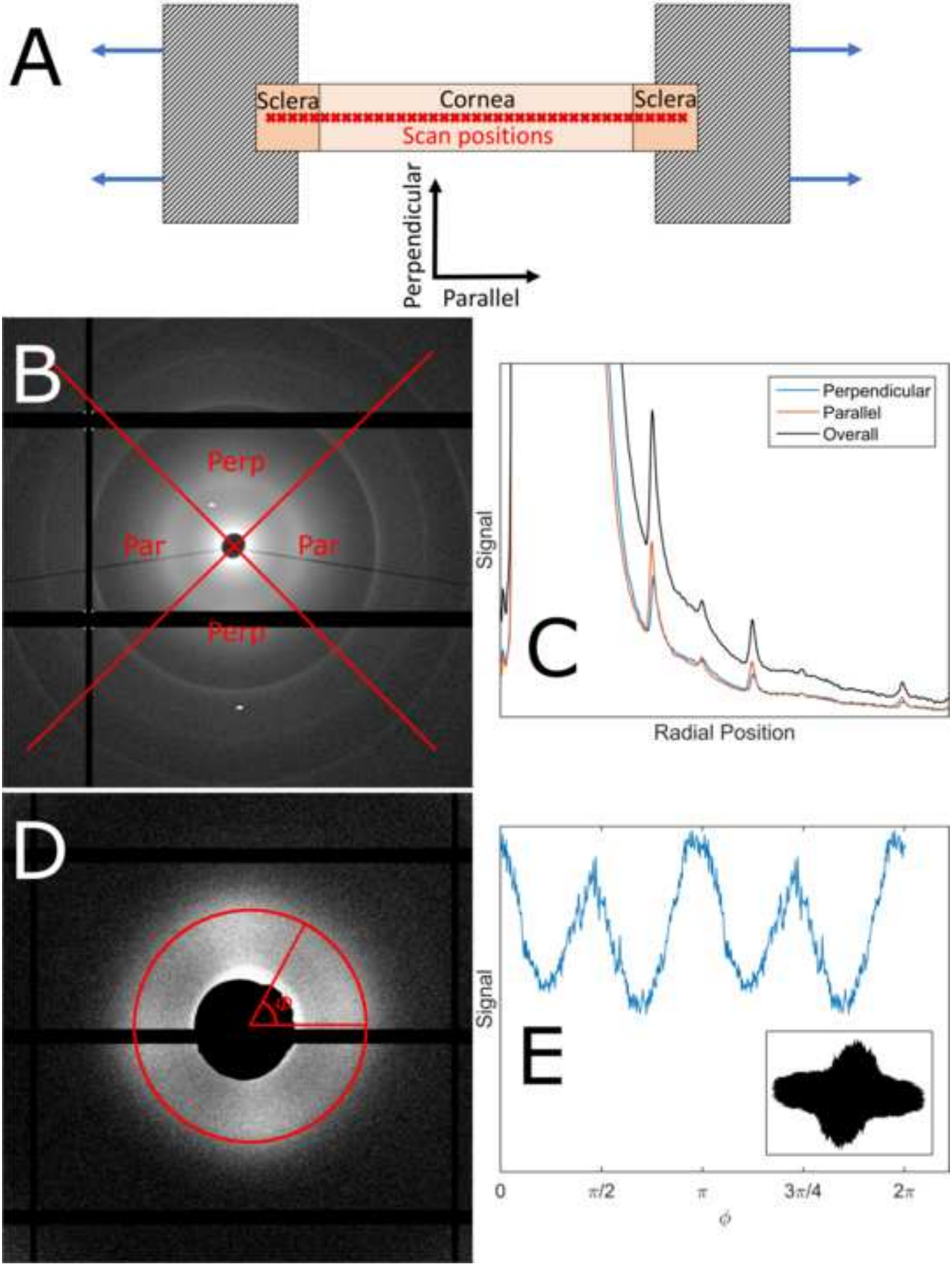

Figure 4
Click here to download high resolution image

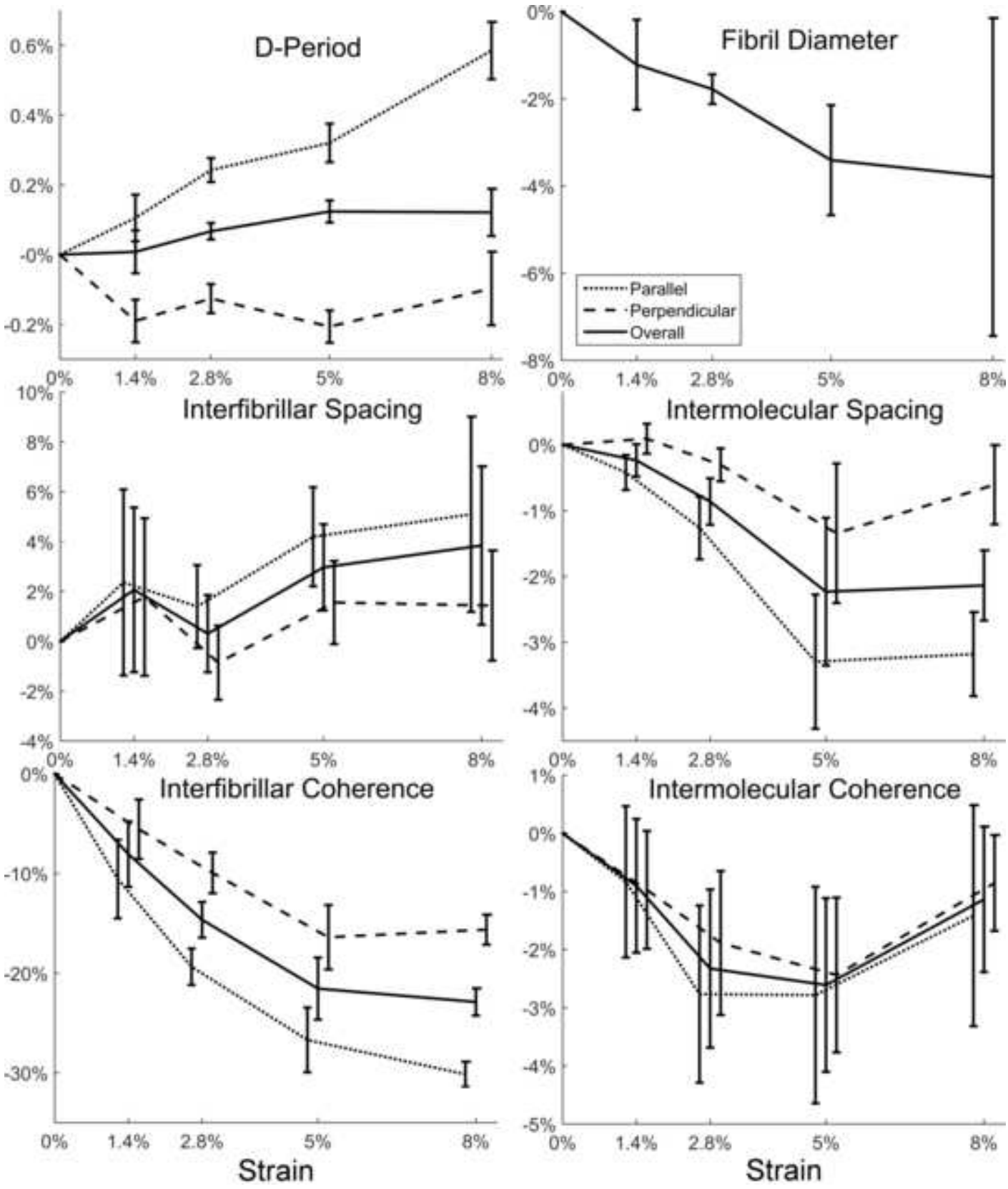

Figure 5

Click here to download high resolution image

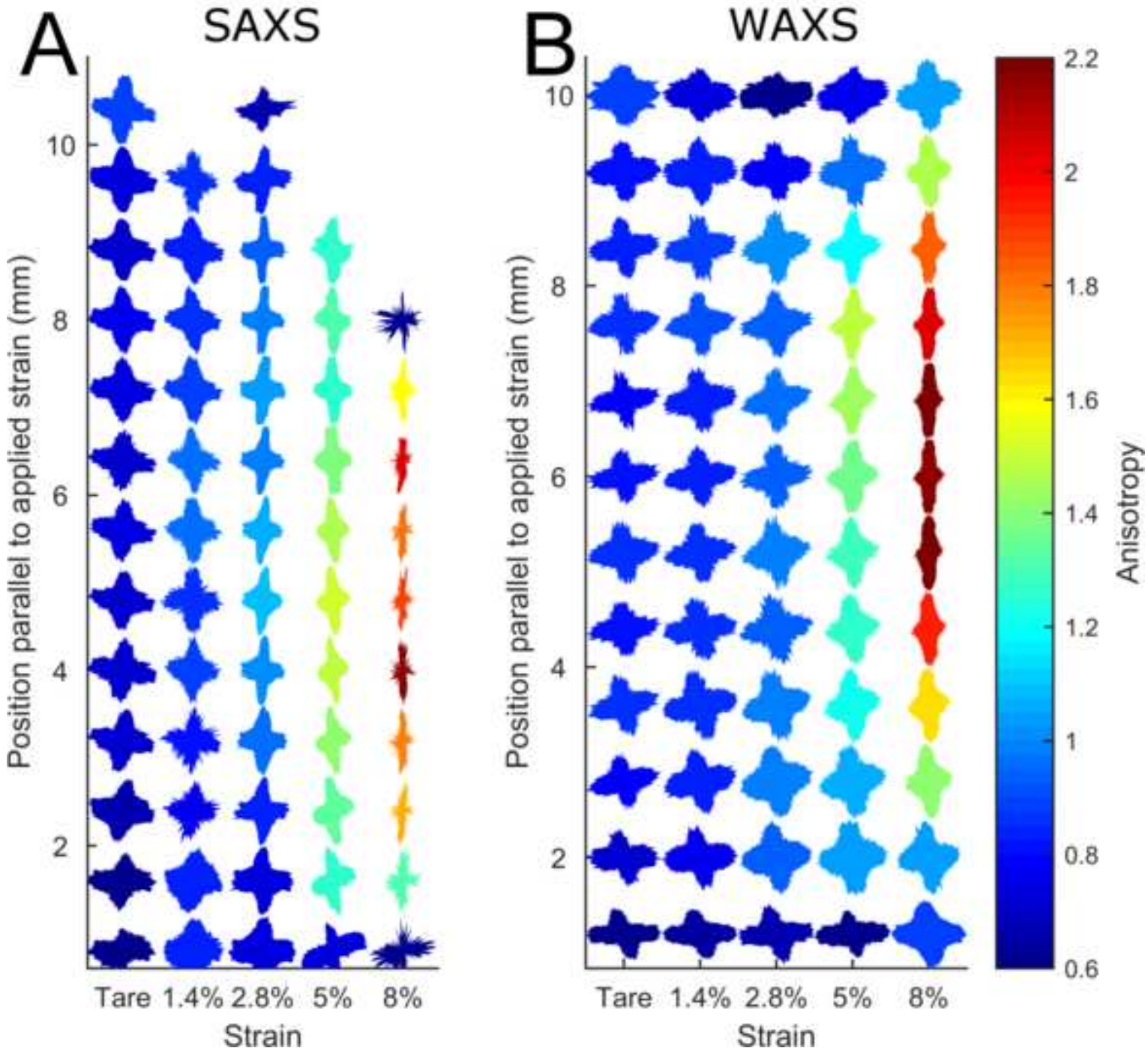

Figure 6

Click here to download high resolution image

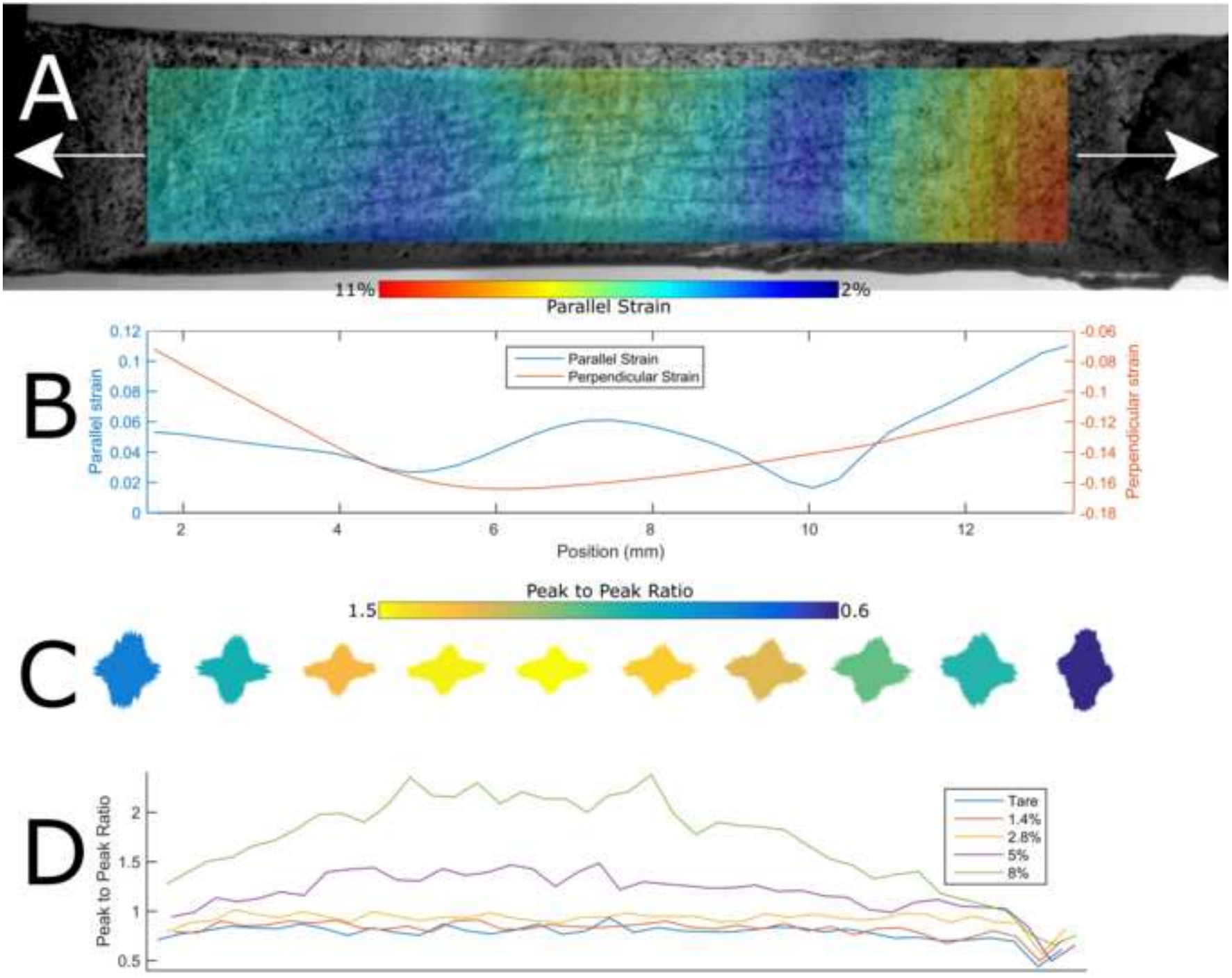

Figure 7

Click here to download high resolution image

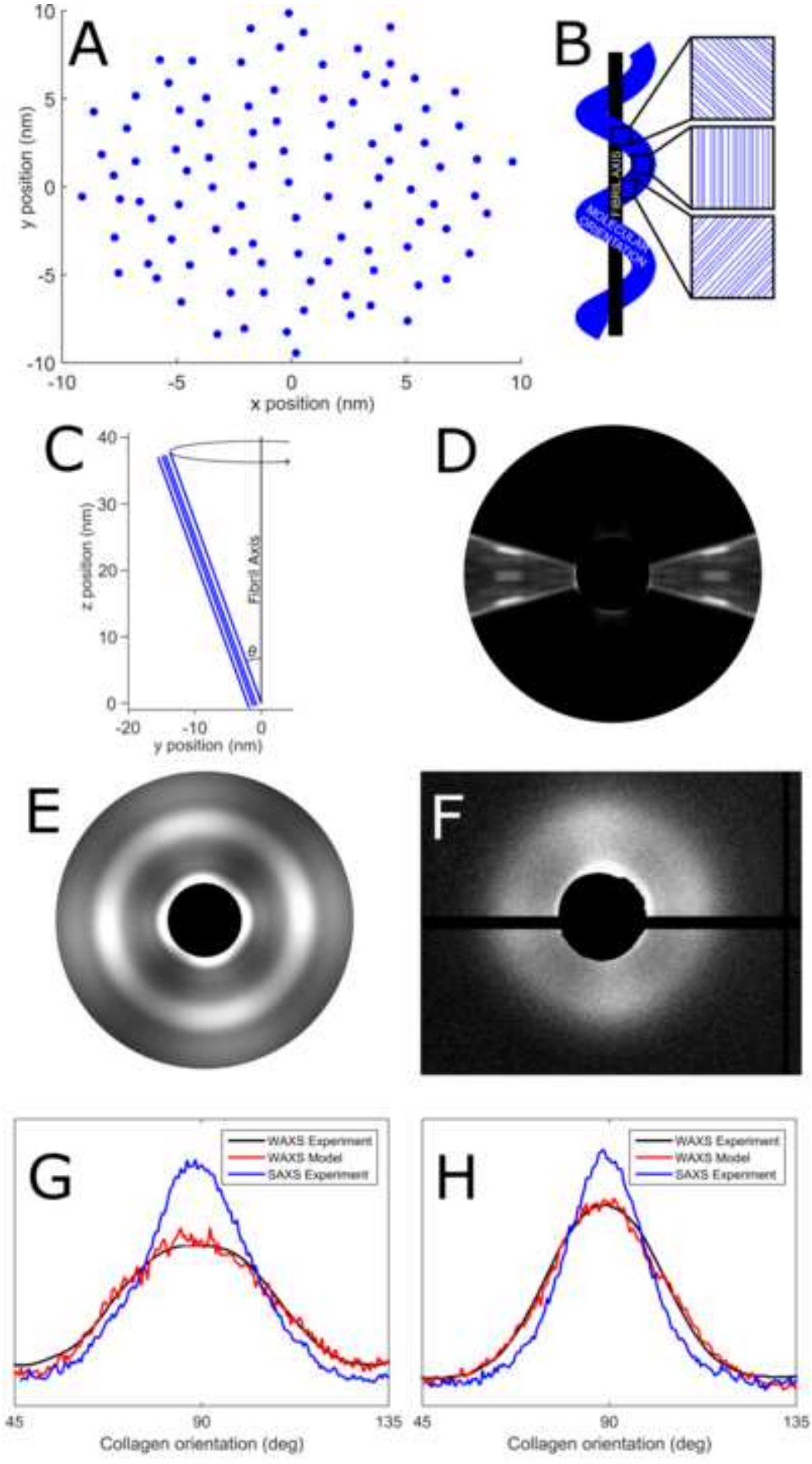

Figure 8
Click here to download high resolution image